Article

Major, Trace and Rare Earth Elements Geochemistry of Bottom Sediments in the Retiro Baixo Reservoir after the B1 Tailings Dam Rupture, Paraopeba River (Brazil)

Diego S Sardinha [1,*], Mateus Sala Pinto [1], Paulo Henrique Bretanha Junker Menezes [1], Gunther Brucha [1], Jéssica Teixeira Silveira [1], Letícia Hirata Godoy [1], Deivid Arimatea Saldanha de Melo [2] and Fernando Verassani Laureano [3]

1   Science and Technology Institute, Alfenas Federal University, Poços de Caldas 37715-400, MG, Brazil
2   Science and Nature Institute, Alfenas Federal University, Alfenas 37130-001, MG, Brazil
3   Vale S/A-Repair Directorate (MG), Nova Lima 34000-000, MG, Brazil
*   Correspondence: diego.sardinha@unifal-mg.edu.br

Abstract: The rupture of an iron mining tailing dam in Brumadinho, Brazil, released around 10 million cubic meters of tailings, of which 1.6 Mm^3 reached the Paraopeba River. In this work, a total of 30 samples from three bottom sediment cores were collected in the lower course of the Paraopeba River basin and analyzed for major, trace and rare earth elements by ICP-OES and ICP-MS. The sediments presented a range of compositions with different weathering histories, overall marked by depleted Ca^{2+}, Na^+ and K^+ compared with the average UCC, PAAS and NASC and some advanced weathering trends. The samples presented a fractionation pattern characterized by a continuous depletion of light REEs from La to Sm and a regular decreased distribution of heavy REEs from Gd to Yb, and the Co/Th vs. La/Sc diagram indicates a predominant intermediate source. The upper samples presented the highest contents of REEs, probably due to the higher presence of iron and aluminum oxides and hydroxides, which can be related to more advanced weathering. The Al, Cu, Ni, V, Zn, Co, Mn, Ti, Fe and Si concentrations and the CF, EF and Igeo index values varied across the sediment core samples, demonstrating that there were long periods of geogenic or anthropogenic contributions.

Keywords: weathering; contamination factor; enrichment factor; geoaccumulation index

1. Introduction

Chemical weathering is an important process that leads to rock alteration, soil formation and leaching solution contribution to the flowing water throughout a drainage basin, especially in hot and humid tropical regions like Brazil. Bedload and suspended sediments are mainly composed by the weathering product mixture delivered along the drainage basins and bear key information on provenance, tectonic setting and weathering mechanism, so they are important objects in the study of supergene geological processes [1,2]. According to [3], geochemical elemental analysis of riverbed sediments can not only reveal the law of element migration during epigenesis but also help to deeply analyze and determine the influence of natural and anthropogenic processes on the distribution of heavy metals in riverbed sediments of the watershed and reduce the regional geochemical process of heavy-metal pollution formation in sediments.

Mining is a human activity capable of generating wealth and social development but, when not properly operated, can be a source of impacts on the landscape and riverbed sediments, which can compromise hydrographic basins and reservoirs. Mine wastes also play a particular role in this context because they represent a source of contamination. The pollution of soil and water by mining deposits has negative effects on both agricultural and tourism land uses; thus, a correct environmental characterization of the affected area is important for any proposal of effective measures that could help to minimize

environmental impact and concern [4–16]. In November 2015, an iron mining tailing dam owned by Samarco Company collapsed in Brazil, releasing an estimated 52 million m^3 of tailings into the environment, affecting the public water supply, which was interrupted for a few weeks, to approximately 400,000 people, as well as industrial activities, electricity generation in three hydroelectric plants, fishing, tourism, and agriculture [17,18].

According to [19,20], riverbed sediments can be used for historical reconstruction of a metal's concentration due to land-use and land-cover change (LULCC) in watersheds. Studies on the major, trace and rare earth elements concentrations in riverbed sediments have been carried out based on different geochemical approaches, such as geoaccumulation index (Igeo), enrichment factor (EF), contamination factor (CF), pollution index (PI), ecological risk factor (Eir), pollution load index (PLI), degree of contamination (Cdeg), modified contamination factor (mCdeg), potential ecological risk index (PERI) and others [21–33].

The geochemistry of the Paraopeba River basin, located in the Iron Quadrangle (IQ), may be related to physiographic factors such as geology; relief; pedology; and human activities, like steel industry, metallurgical, automotive industries, agriculture, livestock farming and mining. Unfortunately, the rupture of the B1 dam in Brumadinho in 2019 on January 25th released around 10 million cubic meters of tailings, which spilled into the Ferro Carvão creek valley, reaching the Paraopeba River. According to [34], the dam reached 86 m high, and it was the main tailing impoundment from an iron ore mining complex named Mina do Córrego do Feijão. After the dam burst, approximately 8.1 Mm^3 was deposited in the Ferro-Carvão creek valley, and 1.6 Mm^3 settled into the Paraopeba River, resulting in a direct impact on channel sediment composition and dynamics. The authors also emphasize that because of geological complexity and historical terrain occupation and usage, geochemical anomalies are common in the Paraopeba River sediments.

The Retiro Baixo reservoir was formed to supply a hydroelectric plant operating since 2010. It is located about 300 km downstream of the mouth of the Ferro Carvão creek, and it is assumed to be the most distal point where the effects of the tailings' alluvial transporting can be measured [35]. The present work aims to evaluate major, trace and rare earth elements of bottom sediments in the Retiro Baixo reservoir after the B1 tailings dam rupture, to be used as a baseline for evaluating environmental impacts that historically accumulate in the Paraopeba River basin in the Minas Gerais state.

2. Study Area

The Paraopeba River basin, with a 12,054 km^2 drainage area, is in the central region of the Minas Gerais state, which consists of 48 municipalities and is home to approximately 1,320,000 inhabitants. The Paraopeba River has its source in the extreme south of Serra do Espinhaço, municipality of Cristiano Otoni, and covers an approximate distance of 510 km to its mouth at the Três Marias dam on the São Francisco River, between the Felixlândia and Pompéu municipalities, being divided in Upper Paraopeba, Medium Paraopeba and Low Paraopeba [36]. The Retiro Baixo reservoir flooded an area of 22.58 km², with a length of 1351.67 m behind a 45 m dam height. It was built between 1973 and 1981 in the Curvelo and Pompeu municipalities to generate hydroelectric power and provide water for agriculture and other uses (Figure 1).

The east border of the watershed partially follows the highlands and ranges of an important Brazilian mineral province, named Quadrilátero Ferrífero (Iron Quadrangle) [37]. According to [38], the Iron Quadrangle is one of the World's richest mineral regions, covering an approximately 7000 km^2 area with important mining activities focused on iron ores and vast reserves of gold, limestone, dolomite, bauxite, steatite, manganese, topaz, clay, etc.

The basin geological substrate is composed of several lithotypes generally associated with Precambrian geotectonic arrangements [39,40]. In the upper and middle Paraopeba, the granite–gneissic rocks from the Belo Horizonte and Bonfim Complexes (Archean), the Archean greenstone belt associated with the Rio das Velhas Supergroup and the Proterozoic metasedimentary units from the Minas Supergroup stand out. In the lower Paraopeba, the Neoproterozoic sedimentary covers from the Paraopeba and Três Marias formations

(Bambuí Group) are highlighted (Figure 2a). Ferralsols and Acrisols are found mainly in the upper and lower parts, followed by Cambisols in the middle Paraopeba basin [41] (Figure 2b). According to [34], the mineral content from the Paraopeba River sediments reflects the weathering of the outcropping rocks from the entire catchment, in which the predominance of quartz, kaolinite and clay minerals reflects granite–gneissic, quartz and iron oxide complexes of the Minas Supergroup, while gibbsite and clay minerals are likely sourced from chemical weathering.
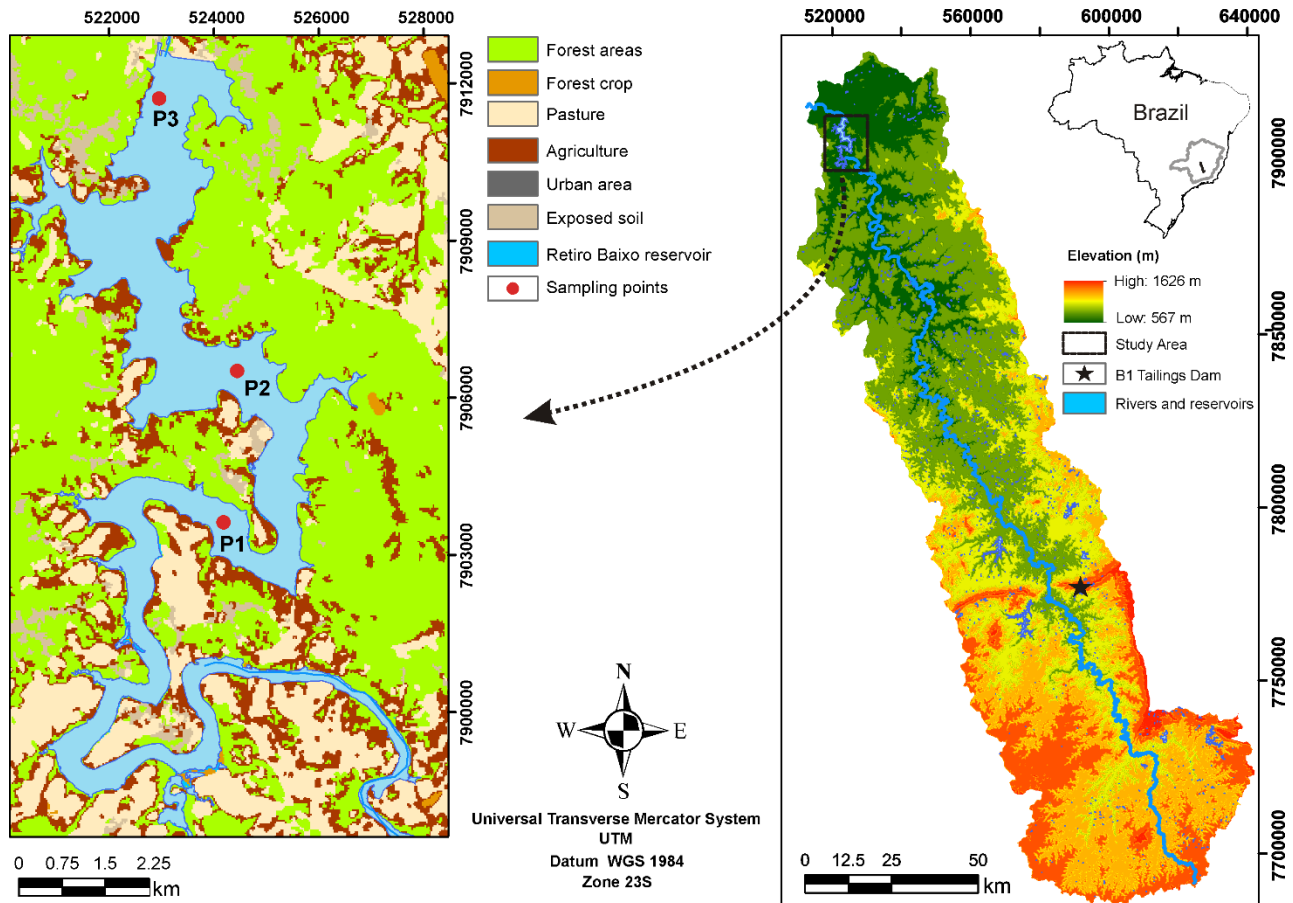

Figure 1. Paraopeba River basin with emphasis on the B1 tailings dam and Retiro Baixo reservoir sampling point locations.

Regarding the B1 tailing dam, it is important to mention that during the lifecycle of the Córrego do Feijão Mine, no metallurgical ore treatment was performed, except those physical processes necessary to achieve particle comminution. According to [42], the B1 tailing dam mineral assemblage is primarily hematite and quartz and secondarily kaolinite and gibbsite, which lead to the mean chemical composition of iron oxides (48%), silica (20.6%), aluminum oxides (3.2%) and manganese oxides (1.0%). Ref. [43] states that the tailings are mostly composed of silts and the natural sediments by fine- to medium-grained sand, with a mineralogical composition that includes hematite, magnetite and manganese oxide, rich in iron (48.7%) and manganese (0.5%) and poor in alumina (3.1%). The natural sediments, according to the authors, are composed of quartz, kaolinite and hematite, meaning that they are rich in silica (59.0%) and alumina (13.1%) and contain some iron (15.2%) and manganese (0.2%).
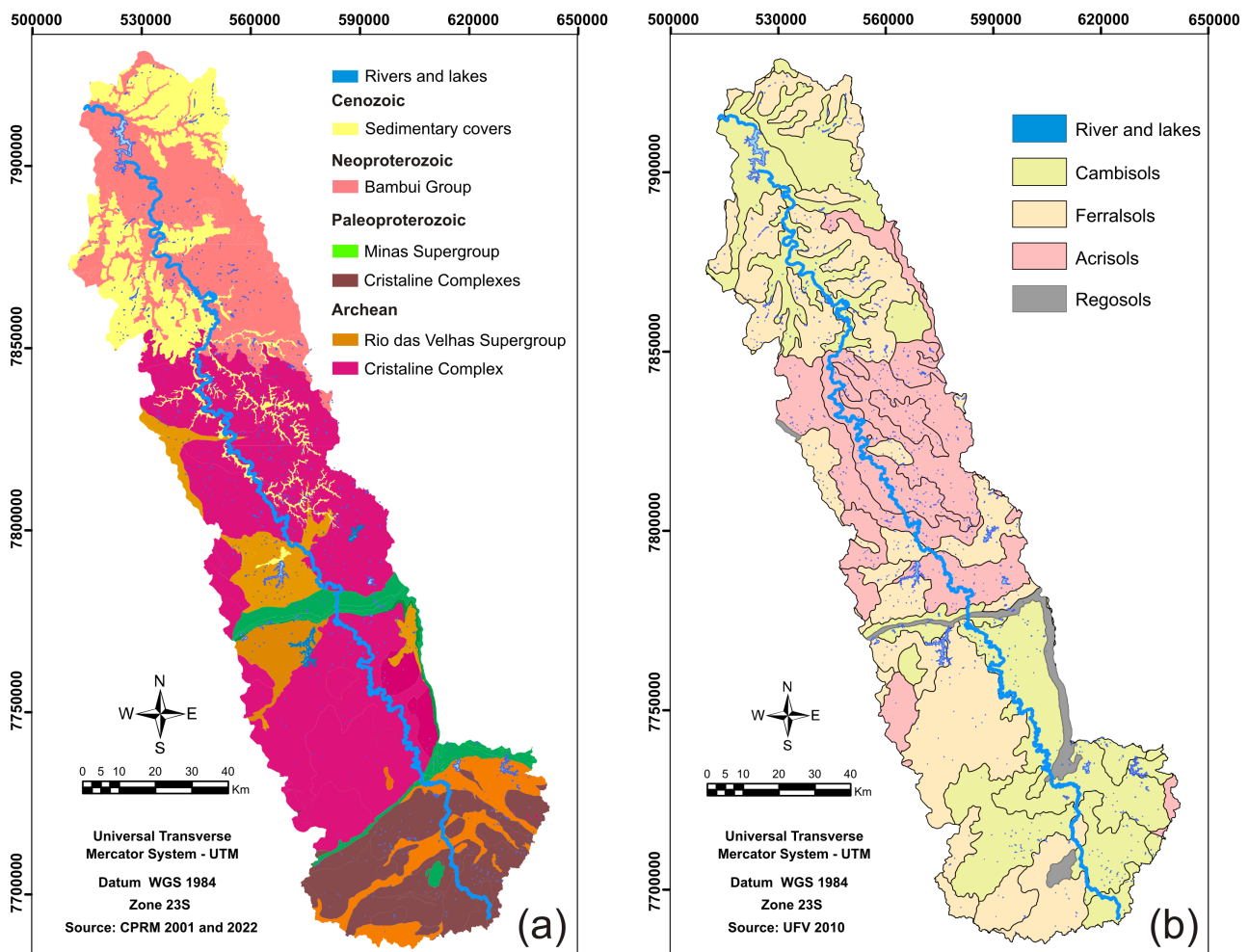
Figure 2. Paraopeba River basin. (**a**) Lithological map. (**b**) Soil map.

3. Materials and Methods

In order to estimate major, trace and rare earth elements in bottom sediment from the lower course of the Paraopeba River basin due to land-use and land-cover changes, the choice of the sampling location was based on the construction of the Retiro Baixo reservoir. Three sediments boreholes were extracted in 2021 on May 5th by using a Kajak Sediment Core sampler at three representative points located within the reservoir (Figure 1): P1 was close to the beginning or river zone (15 samples from 5 to 75 cm), at the water depth of 9.07 m; P2 was in the central region or intermediate zone (10 samples from 5 to 50 cm), at the water depth of 12.17 m; and P3 was close to the spillway or lake area (5 samples from 8 to 26 cm), at the water depth of 21.77 m. The near-surface and deeper layers of the sediment core were discarded due to the likely mechanical mixing in the first and last few centimeters of the core. Samples were sequentially labeled from top to bottom.

The samples were delivered to SGS Geosol laboratories, responsible for the geochemical analysis. Sample preparation included drying to 105 °C, crushing to 3 mm, homogenization, and quarrying and spraying from 250 to 300 g in a 95% 150 mesh steel mill. The major oxides (SiO_2, TiO_2, Al_2O_3, Fe_2O_3, MnO, MgO, CaO, Na_2O, K_2O and P_2O_5), trace elements and rare earths (Cu, V, Zn, Ni, Tl, Co, Sc, Rb, Ga, Ce, La, Nd, Sm, Th, W, Yb, Gd, Eu, Er, Dy, Cs, Hf, Ho, Lu, Nb, Pr, Tb, Tm, U and Y) were determined by fusion with lithium metaborate ($LiBO_2$) by using inductively coupled plasma optical emission spectrometry (ICP-OES) and inductively coupled plasma mass spectrometry (ICP-MS). Quality control was performed by analyzing duplicate and blank samples to check for precision, whereas accuracy was obtained by using Certified Reference Materials (STD

SG_142, STD SG_241, STD SG_127, STD GRE-03 and STD-GRE-04). Detection limits for the analyzed elements were 0.01% for major oxides; 10.0 ppm for Ba, Zr and Sr; 5.0 ppm for Cu, V, Zn and Ni; 0.5 ppm for Tl, Co and Sc; 0.2 ppm for Rb; 0.1 ppm for Ga, Ce, La, Nd, Sm, Th, W and Yb; and 0.05 ppm for Gd, Eu, Er, Dy, Cs, Hf, Ho, Lu, Nb, Pr, Tb, Tm, and U.

The chemical index of weathering (CIW) in molecular proportions and the index of compositional variability (ICV) [44,45] were calculated for all the samples according to Equations (1) and (2).

$$CIW = \left[\frac{Al_2O_3}{(Al_2O_3 + CaO + Na_2O)} \right] \times 100 \tag{1}$$

$$ICV = \left[\frac{(Fe_2O_3 + K_2O + Na_2O + CaO + MgO + MnO + TiO_2)}{Al_2O_3} \right] \times 100 \tag{2}$$

For data interpretation, the trace elements were normalized by the North American shale composition (NASC) [46], and the REE concentrations were normalized by the CC1 chondrite composition [47,48]. To characterize the REE distribution spectrum, the cerium europium (Eu_n) anomaly values and the light REE-to-heavy REE ratio (LREE/HREE) were calculated according to Equation (3).

$$\frac{E_u}{E_{u^*}} = \frac{Eu_n}{(Sm_n \times Gd_n)^{0.5}} \tag{3}$$

Contamination factor (CF) determination was performed according to Equation (4). The CF corresponds to the pollution over a period for a given metal [49]. In addition, to assess the environmental impacts or baseline for the historical major and trace elements accumulated in Retiro Baixo reservoir bottom sediments, Equation (5) was used to calculate the enrichment factor (EF). The EF is used as a measure of geochemical trends to compare areas and to identify metals' origin and contamination [19,24]. In addition, to assess the degree of pollution of the metals studied in the Retiro Baixo reservoir, the geoaccumulation index (Igeo), introduced by [50], was used (Equation (6)). According to [51], to consider the variations in the amount of mineral material in the major and trace elements concentration profiles, the elements concentrations were normalized to Sc, which is a conservative metal with no significant anthropogenic source.

$$CF = \frac{[M]_{sed}}{M_{ref}} \tag{4}$$

$$EF = \frac{\left(Mi / Sc \right)_{sample}}{\left(Mi / Sc \right)_{ref}} \tag{5}$$

$$I_{geo} = Log_2 \frac{[M]_{sed}}{1.5 . M_{ref}} \tag{6}$$

where $[M]_{sed}$ is the metal element concentration M in the sediment and $[M]_{ref}$ is the same metal element concentration M in the geochemical background reference; $(Mi/Sc)_{sample}$ is the ratio between the metal concentration (Mi) and Sc in the sediment sample; $(Mi/Sc)_{ref}$ corresponds to the ratio between the metal concentration (Mi) and Sc of the reference geochemical background.

The anthropogenic contribution status was evaluated by comparing the collected data to a background that involves regional or natural geochemical data. Thus, the major and trace element concentrations (Si, Ti, Al, Fe, Mn, V, Co, Ni, Cu and Zn) measured by [52] in two sediment samples from the upstream Córrego do Feijão Mine, the Paraopeba River and Sc relative to the upper continental crust (UCC) [53,54] were used for comparison.

4. Results and Discussion

4.1. Major Elements

The major oxide element contents of sediments in the Retiro Baixo reservoir are listed in Table 1, and the concentrations are compared with the average North American shale

(NASC) [46,55], Average Post-Archaean Australian Shale (PAAS) and upper continental crust (UCC) [53,54]. The SiO_2 content varies from 35.8 to 72.1%, with the average value of 41.6%, among the bottom sediments. Along with each profile (P1, P2 and P3), these values slightly decrease from lower to upper levels. The SiO_2 content in the samples is attributed mainly to the presence of clay minerals and quartz, and it varies according to the weathering hydrolysis reaction evolution. The smallest contents of this oxide are found in the sample from P2–10 cm (35.8%; Table 1).

Table 1. Major oxide chemical composition of bottom sediments in Retiro Baixo reservoir (wt.%).

		SiO_2	Al_2O_3	Fe_2O_3	MgO	CaO	K_2O	Na_2O	MnO	TiO_2	P_2O_5	LOI	Sum	CIW	ICV
	NASC	64.80	16.90	5.65	2.86	3.63	3.97	1.14	0.06	0.70	0.13	--	--	65.96	1.06
	PASS	62.80	18.90	7.22	2.20	1.30	3.70	1.20	0.11	1.00	0.16	6.00	--	80.89	0.88
	UCC	66.00	15.20	5.00	2.20	4.20	3.40	3.90	0.08	0.50	--	--	--	51.24	1.26
P1	−5 cm	37.88	28.26	11.39	0.55	0.23	1.46	0.10	0.32	0.89	0.18	14.77	96.03	97.92	0.52
	−10 cm	37.05	27.72	13.29	0.52	0.19	1.39	0.09	0.37	0.87	0.23	14.64	96.36	98.20	0.59
	−15 cm	37.04	27.56	14.81	0.53	0.17	1.38	0.08	0.36	0.87	0.20	14.31	97.31	98.38	0.65
	−20 cm	38.51	25.55	15.17	0.54	0.26	1.40	0.11	0.44	0.83	0.21	13.93	96.95	97.43	0.72
	−25 cm	37.55	25.61	14.22	0.52	0.21	1.48	0.09	0.46	0.80	0.23	14.17	95.34	97.91	0.68
	−30 cm	38.25	27.26	11.91	0.54	0.17	1.61	0.09	0.24	0.85	0.22	14.45	95.59	98.30	0.56
	−35 cm	38.61	27.50	11.79	0.56	0.17	1.63	0.10	0.16	0.89	0.21	14.52	96.14	98.26	0.55
	−40 cm	40.98	27.14	12.14	0.57	0.19	1.65	0.10	0.12	0.90	0.21	14.28	98.28	98.10	0.57
	−45 cm	39.39	27.40	11.59	0.54	0.31	1.56	0.10	0.10	0.89	0.18	13.98	96.04	97.34	0.55
	−50 cm	40.44	25.98	12.71	0.54	0.20	1.36	0.13	0.22	0.88	0.17	13.59	96.22	97.76	0.61
	−55 cm	41.03	24.89	12.19	0.54	0.20	1.39	0.13	0.22	0.84	0.15	13.42	95.00	97.67	0.61
	−60 cm	40.76	25.92	12.18	0.54	0.20	1.48	0.12	0.22	0.85	0.16	13.55	95.98	97.82	0.59
	−65 cm	40.72	25.89	11.55	0.52	0.17	1.47	0.12	0.14	0.88	0.17	13.71	95.34	98.03	0.57
	−70 cm	58.92	15.36	10.69	0.40	0.17	1.47	0.26	0.10	0.79	0.09	8.55	96.80	95.30	0.90
	−75 cm	64.90	11.40	10.25	0.35	0.17	1.47	0.32	0.09	0.75	0.06	6.59	96.35	92.99	1.17
P2	−5 cm	41.21	26.89	11.12	0.42	0.13	1.13	0.09	0.21	0.75	0.20	14.91	97.06	98.55	0.51
	−10 cm	35.82	28.17	13.50	0.45	0.11	1.23	0.09	0.24	0.84	0.22	15.45	96.12	98.74	0.58
	−15 cm	36.77	29.05	11.73	0.43	0.10	1.21	0.07	0.11	0.80	0.22	16.03	96.52	98.96	0.49
	−20 cm	36.80	28.72	11.36	0.45	0.10	1.26	0.08	0.09	0.82	0.23	16.04	95.95	98.89	0.49
	−25 cm	37.83	28.80	10.77	0.46	0.10	1.33	0.08	0.07	0.83	0.23	16.27	96.77	98.89	0.47
	−30 cm	37.95	28.80	10.49	0.46	0.11	1.32	0.06	0.06	0.84	0.23	16.12	96.44	98.94	0.46
	−35 cm	37.92	29.32	10.78	0.47	0.10	1.29	0.08	0.11	0.87	0.18	15.86	96.98	98.91	0.46
	−40 cm	37.83	28.68	10.32	0.48	0.11	1.35	0.08	0.13	0.85	0.18	15.43	95.44	98.82	0.46
	−45 cm	50.50	22.66	7.99	0.41	0.09	1.17	0.07	0.07	0.80	0.15	12.74	96.65	98.75	0.46
	−50 cm	72.10	11.95	4.34	0.28	0.06	0.83	0.04	0.03	0.73	0.08	7.02	97.46	98.52	0.53
P3	−8 cm	36.88	27.53	11.58	0.42	0.16	1.11	0.06	0.14	0.77	0.22	16.52	95.39	98.56	0.51
	−16 cm	36.97	28.58	11.11	0.42	0.13	1.20	0.06	0.11	0.76	0.22	16.39	95.95	98.81	0.48
	−24 cm	39.11	29.07	11.20	0.45	0.12	1.30	0.06	0.11	0.80	0.21	16.16	98.59	98.89	0.48
	−32 cm	38.47	29.81	10.63	0.45	0.09	1.25	0.07	0.12	0.84	0.19	15.41	97.33	99.05	0.45
	−36 cm	39.87	28.57	10.52	0.46	0.10	1.32	0.06	0.11	0.83	0.18	15.61	97.63	99.00	0.47

UCC: upper continental crust; PAAS: Average Post-Archaean Australian Shale; NASC: Average North American Shale Composite. CIW: chemical index of weathering; ICV: index of compositional variability.

Al_2O_3 varies between 11.4 and 29.8% with an average of 26.0% among the samples; this is a common oxide in minerals such as kaolinite ($Al_2Si_2O_5(OH)_4$) and gibbsite ($Al(OH)_3$). Among the profiles, Al_2O_3 content presents an opposite behavior when compared with SiO_2 because of increased Si mobility. Fe_2O_3, TiO_2 and MnO oxides and the loss on ignition (LOI) also increase upward and vary between 4.3 and 15.2% (11.4% average), 0.7 and 0.9% (0.8% average), 0.03 and 0.46% (0.18% average) and 6.6 and 16.5% (14.1 average), respectively (Table 1). These elements may be related to hematite (Fe_2O_3), magnetite (Fe_3O_4) and manganese oxide (MnO_2) minerals. The B1 tailing dam presents a mean chemical composition marked by iron oxides (48%), silica (20.6%), aluminum oxides (3.2%) and manganese oxides (1.0%) [42]. According to [43], the tailings' composition is rich in iron

(48.7%) and manganese (0.5%) and poor in alumina (3.1%), and the natural sediments are composed by silica (59.0%), alumina (13.1%), some iron (15.2%) and manganese (0.2%).

Following [2], hydrological/sedimentary processes such as sorting and recycling may be of particular importance in modifying the relative mineral abundances and consequently the concentrations of specific elements, and in the upper continental crust chemical weathering process, a great surface fluid loss of alkali metal elements such as Na_2O, K_2O and CaO occurs as ions and forming clay minerals (e.g., kaolinite, illite and smectite). MgO and P_2O_5 occur in minor proportions and vary across the profiles.

The Al_2O_3-CaO+Na_2O+K_2O-Fe_2O_3+MgO (A-CNK-FM) ternary diagram [56–58] is used to access the weathering trends. The studied sediment samples present a range of compositions that are plotted along the A-axis (Figure 3A), suggesting different weathering histories with depletion of Ca^{2+}, Na^+ and K^+ compared with the average upper continental crust (UCC), Average Post-Archaean Australian Shale (PAAS) and Average North American Shale Composite (NASC). In these samples, the relative increase in Al_2O_3 and Fe_2O_3 may be related to the iron and aluminum oxides and hydroxides. But P1 (75 and 70 cm) samples are in a different group, closest to illite and muscovite, as shown in Figure 3A.
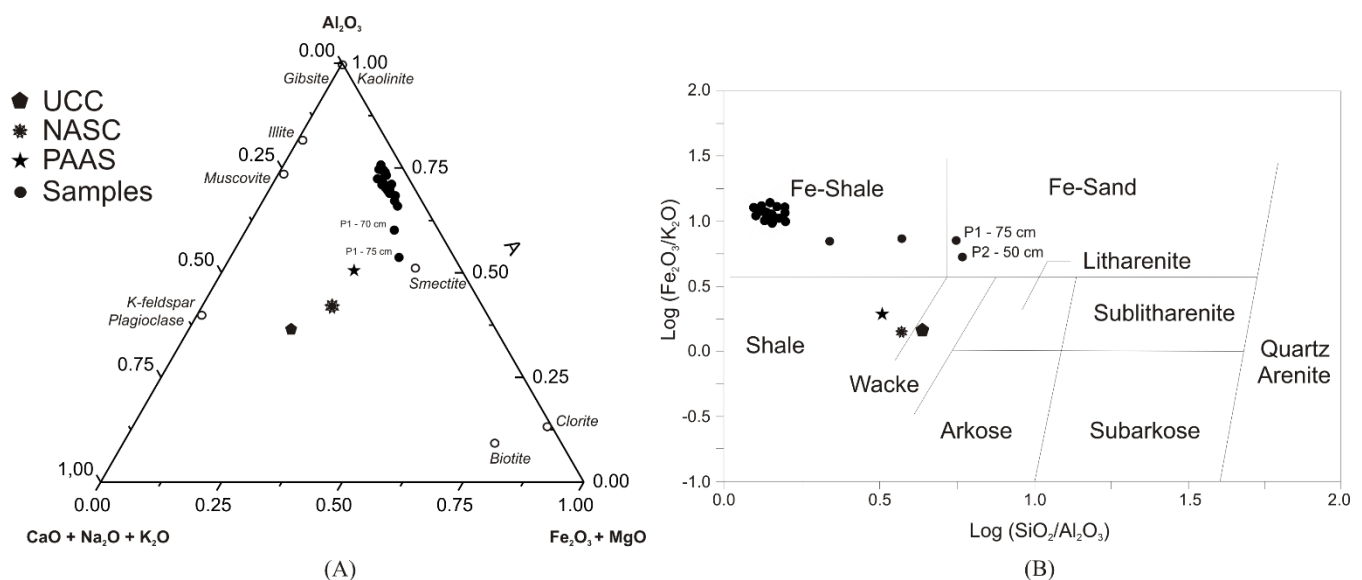

Figure 3. (**A**) The ternary diagram of the $(Al_2O_3)/(CaO+Na_2O)/(K_2O)$ oxides, in molecular proportions, for the bottom sediment samples [56–58]. (**B**) The classification of terrigenous sandstones and shales using Log (Fe_2O_3/K_2O) vs. Log (SiO_2/Al_2O_3) [59].

The chemical index of weathering (CIW) and index of compositional variability [44,45] are calculated for all the samples, and show similar patterns (Table 1) that correlate to the observations made in the A-CNK-FM diagram (Figure 3A). The highest values for the CIW, 99.0 ± 1.2, corresponds to the samples located in the advanced weathering trend, for sediment samples from P1, P2 and P3. Immature sediments, containing a high proportion of silicates other than clays, commonly show high values of this index (ICV > 1), whereas mature sediments, depleted in silicates other than clays, generally show low ICV values (ICV < 1). The ICV values vary between 0.45 and 1.17, with only one exception >1 (P1 = 75 cm). This suggests an advanced weathering trend, like the CIW and the A-CNK-FM diagram (Figure 3A).

The classification diagram of terrigenous sandstones and shales was used with log (Fe_2O_3/K_2O) vs. log (SiO_2/Al_2O_3) (Ref. [59]—Figure 2B). According to [2], the sediment compositional maturity is mainly used to reflect degrees of clastic material altered during the processes of weathering and transport trend to final products. As long as sediment maturity increases, there is an increase in quartz content at the expense of feldspar and in lithic fragments in the sediments. All samples nearly fall into the Fe-Shale and Fe-Sand

region, indicating that the chemical maturity of these sediments is highly weathered. Samples with very high Fe_2O_3/K_2O ratios (>4) are classified as iron-rich or ferruginous and are further broken down as Fe-rich sands or Fe-rich shales [59].

4.2. Trace and Rare-earth Elements (REEs)

The samples' trace element contents, including REEs, are listed in Table 2, and the concentrations are compared with the average North American Shale (NASC) [46,58], Average Post-Archaean Australian Shale (PAAS), upper continental crust (UCC) [53,54] and CC1 chondrites [47,48]. The data normalized to NASC from [46] and to CC1 chondrites [47,48] are plotted in distribution diagrams according to each profile (Figure 4).

The Sc, Co, Ni, Rb, Cs, Ba, La, Ce, Pr, Nd, Sm, Eu, Gd, Tb, Dy, Ho, Er, Tm, Yb, Lu, Th and U concentrations increase from the deepest layers to the top ones, mainly in P1 and P2; the values of Sr and W are practically constant, with differences between the depths of −30 cm in P1 and −15 and in P2, and there is a decrease in Zr and Hf from the deeper layers to the top ones. The depletion of the Rb, Sr and Ba elements in the bottom sediments relative to UCC, PASS and NASC can be noticed. Compared with UCC, PASS and NASC, La, Ce, Pr, Nd, Sm, Th and U are slightly enriched, particularly in the upper layers. Cs is enriched in sampled sediments relative to the UCC, but it is depleted in most of the sediments relative to PAAS (Figure 4 and Table 2).

Samples P1 and P2 at depths of 35 cm and 20 cm, respectively, are strongly enriched in W relative to NASC, which may be due to the concentration of iron–manganese minerals. The samples of P1 (70 and 75 cm) and P2 (50 cm) are strongly enriched in Zr and Hf relative to PAAS and UCC, which may be due to the concentration of certain accessory minerals. Although higher than UCC, NASC and PASS in most samples, Ni concentrations in samples P1 (10 cm) and P3 (24 cm) may be associated with the crystalline structure of some ferromagnesian minerals. For Ba, Ce, Nd, Sm and Yb, sample P3 (36 cm) concentrations are well below the reference UCC, NASC and PASS levels. All the samples present a positive anomaly for Cs, and according to [60], because of this element's mobility (low charge and large ionic radius) during the weathering processes, it is more easily carried out the system by the weathering fluids. Another important point is the contraction of Co at the depth of −24 cm at point P3 and the increase in Th and U concentrations at all points, especially in the deeper samples (Figure 4), which is probably associated to accessory minerals.

In Figure 5, one can notice that samples from P1, P2 and P3 show an REE element increase from the bottom to the upper portions. The average ranking of concentrations is as follows: Ce > La > Nd > Pr > Sm > Gd > Dy > Er > Yb > Eu > Ho > Tb > Tm > Lu, ranging from 99.35 mg/kg for Ce to 0.38 mg/kg for Lu. The REE average concentrations in sediments from the deepest layers of the three sampling points were normalized by using CC1 Chondrite, and different general pattern and enrichment were observed; however, the ranking of concentrations was similar. The highest patterns were for P2 (−30 cm), and the lowest one was for P1 (−75 cm) according to the normalization method (Figure 4 and Table 3).

Bottom sediment samples present an average REE concentration of $\sum REE_n$ = 751.58 mg/kg ± 113.15 and a fractioning pattern characterized by a continuous depletion in light REEs from La to Sm (La/Sm_{cn} = 4.27 ± 0.19) and a regular decreased distribution of heavy REEs from Gd to Yb (Gd/Yb_{cn} = 1.85 ± 0.22). However, the average concentration of REEs in the P1 upper portions −5 to −65 cm (ΣREE = 759.86 mg/kg ± 38.17) is higher than in the lower portions −70 to −75 cm (ΣREE = 438.01 mg/kg ± 43.53). The upper samples present the highest contents of REEs, probably due to the higher presence of iron and aluminum oxides and hydroxides, which can be related to the more advanced weathering state of these samples (Figure 3).

Table 2. Trace and rare earth elements concentrations in sediments (mg/kg).

		Sc	Ni	Co	V	Zn	Cu	Rb	Sr	Zr	Cs	Ba	La	Ce	Pr	Nd	Sm	Eu	Gd	Tb	Dy	Ho	Er	Tm	Yb	Lu	Hf	W	Th	U
	NASC	14.90	58.00	25.70	130.00	2.70	--	125.00	142.00	200.00	5.16	636.00	31.10	67.03	7.90	30.40	5.98	1.25	5.50	0.85	5.54	1.04	3.28	0.50	3.11	0.46	6.30	2.10	12.3	2.66
	PASS	16.00	55.00	23.00	150.00	85.00	50.00	160.00	200.00	210.00	15.00	650.00	38.20	79.60	8.83	33.90	5.55	1.08	4.66	0.77	4.68	0.99	2.85	0.41	2.82	0.43	--	--	3.10	--
	UCC	11.00	20.00	10.00	60.00	71.00	25.00	110.00	350.00	240.00	3.70	700.00	30.00	64.00	7.10	26.00	4.50	0.88	3.80	0.64	3.50	0.80	2.30	0.33	2.20	0.32	5.80	--	10.50	2.50
	CC1	--	9.90	--	--	--	--	2.32	--	--	0.18	2.41	0.24	0.64	0.09	0.47	0.15	0.06	0.20	0.04	0.25	0.06	0.17	0.03	0.16	0.02	--	--	0.03	0.01
P1	−5 cm	19.20	63.00	19.60	111.00	102.00	50.00	96.10	36.00	112.00	4.82	479.00	48.10	97.10	9.72	34.90	7.20	1.52	6.05	0.84	4.83	0.91	2.58	0.38	2.40	0.36	3.38	5.00	27.00	10.52
	−10 cm	21.40	82.00	36.90	114.00	100.00	55.00	87.80	26.00	114.00	4.87	479.00	49.00	103.40	10.23	35.90	7.00	1.64	6.49	0.91	5.17	1.01	2.82	0.40	2.70	0.41	3.37	2.60	26.70	11.13
	−15 cm	21.10	67.00	21.90	100.00	100.00	60.00	79.90	37.00	119.00	4.51	481.00	46.10	99.60	9.80	34.90	7.10	1.66	6.02	0.88	5.14	0.99	2.85	0.41	2.70	0.39	3.29	2.30	24.10	11.15
	−20 cm	19.30	65.00	20.30	92.00	108.00	61.00	82.70	39.00	159.00	4.53	483.00	47.90	106.60	10.40	37.20	7.30	1.64	6.61	0.93	5.34	1.05	3.08	0.45	2.90	0.42	4.32	2.50	23.30	10.54
	−25 cm	19.90	67.00	25.20	98.00	98.00	57.00	89.60	38.00	123.00	5.12	460.00	48.10	102.00	10.59	37.50	7.50	1.69	6.85	0.98	5.67	1.11	3.23	0.47	3.10	0.44	3.69	2.60	24.50	11.11
	−30 cm	21.40	67.00	23.00	103.00	85.00	54.00	100.00	34.00	118.00	5.85	467.00	49.80	99.50	10.76	38.00	7.90	1.71	6.33	0.93	5.33	1.06	2.91	0.40	2.80	0.42	3.75	3.20	25.60	10.34
	−35 cm	23.40	64.00	18.50	128.00	86.00	95.00	93.80	31.00	130.00	5.21	465.00	48.70	98.90	10.19	36.50	7.10	1.52	6.10	0.84	5.10	0.99	2.69	0.38	2.60	0.38	3.80	11.30	25.50	9.06
	−40 cm	23.40	59.00	16.60	123.00	88.00	66.00	92.70	32.00	150.00	5.11	470.00	50.70	106.20	10.54	37.80	7.40	1.55	6.35	0.88	4.92	0.99	2.90	0.41	2.80	0.39	4.33	3.20	26.20	9.41
	−45 cm	23.10	60.00	16.90	136.00	92.00	60.00	88.30	31.00	130.00	4.74	457.00	50.40	101.90	10.43	36.90	7.10	1.56	6.26	0.88	5.11	0.98	2.77	0.41	2.60	0.39	4.04	2.40	26.60	9.91
	−50 cm	22.80	68.00	23.00	116.00	91.00	51.00	80.40	31.00	180.00	4.02	445.00	49.70	107.10	10.41	36.60	7.10	1.54	6.14	0.88	5.06	0.96	2.80	0.39	2.60	0.39	5.08	2.70	25.80	9.58
	−55 cm	22.00	61.00	21.90	95.00	96.00	46.00	81.90	30.00	195.00	4.15	442.00	45.50	96.70	9.57	34.20	6.40	1.46	5.83	0.79	4.72	0.88	2.51	0.36	2.50	0.36	5.24	2.10	23.00	9.05
	−60 cm	22.10	61.00	20.40	93.00	89.00	44.00	84.80	30.00	176.00	4.20	454.00	45.20	95.00	9.36	33.80	6.20	1.37	5.35	0.75	4.50	0.90	2.57	0.37	2.40	0.34	4.70	2.30	24.30	9.00
	−65 cm	24.80	62.00	19.10	113.00	96.00	48.00	82.00	31.00	180.00	4.02	467.00	43.40	90.90	9.04	31.90	6.20	1.40	5.44	0.77	4.35	0.87	2.60	0.35	2.50	0.33	4.85	4.60	23.10	9.09
	−70 cm	14.60	38.00	12.70	61.00	59.00	28.00	65.10	39.00	366.00	2.65	419.00	27.90	59.00	6.06	21.70	4.30	0.93	3.97	0.56	3.44	0.68	2.10	0.30	2.10	0.32	8.98	1.50	15.60	6.07
	−75 cm	11.50	33.00	8.30	47.00	46.00	20.00	60.10	42.00	415.00	2.12	392.00	24.90	51.00	5.23	18.60	3.70	0.76	3.26	0.48	2.95	0.60	1.79	0.27	1.90	0.28	10.06	1.60	13.60	5.35
P2	−5 cm	18.60	58.00	15.00	96.00	93.00	47.00	73.70	25.00	86.00	4.97	368.00	48.00	99.40	10.13	35.90	7.00	1.49	6.03	0.83	4.75	0.91	2.57	0.36	2.50	0.36	2.88	1.90	23.90	9.25
	−10 cm	21.20	67.00	17.00	100.00	104.00	51.00	80.60	31.00	102.00	5.10	414.00	50.80	105.10	10.87	37.90	7.60	1.70	6.53	0.95	5.41	1.02	2.87	0.40	2.70	0.39	3.14	2.00	25.10	10.75
	−15 cm	21.20	61.00	13.90	111.00	90.00	51.00	77.30	24.00	112.00	5.66	350.00	51.30	109.00	11.15	39.90	7.90	1.73	6.62	0.93	5.43	1.04	2.85	0.40	2.70	0.39	3.33	2.00	25.30	8.78
	−20 cm	22.50	70.00	14.50	125.00	83.00	52.00	80.90	23.00	115.00	5.66	357.00	50.50	110.00	10.95	39.60	7.60	1.58	6.48	0.89	5.21	0.99	2.87	0.43	2.70	0.41	3.50	12.60	26.40	8.92
	−25 cm	21.70	62.00	16.10	142.00	92.00	50.00	90.60	23.00	122.00	6.11	366.00	52.90	115.70	11.62	41.40	8.30	1.76	6.66	0.94	5.56	1.04	2.98	0.41	2.80	0.39	3.77	2.10	26.90	8.46
	−30 cm	21.60	60.00	15.60	159.00	83.00	220.00	85.40	23.00	118.00	5.65	357.00	55.10	114.80	11.97	42.30	8.00	1.72	7.09	0.94	5.39	1.02	2.99	0.41	2.70	0.40	3.58	2.90	27.90	8.73
	−35 cm	22.20	57.00	14.40	149.00	86.00	45.00	79.70	23.00	109.00	4.75	374.00	55.20	114.20	11.46	40.10	7.70	1.65	6.80	0.93	5.19	0.97	2.78	0.37	2.60	0.36	3.28	2.30	29.90	9.99
	−40 cm	22.40	69.00	15.40	119.00	89.00	47.00	89.00	25.00	112.00	4.88	388.00	50.20	105.10	10.58	37.10	7.40	1.56	6.01	0.84	4.81	0.92	2.71	0.37	2.40	0.38	3.40	1.90	28.40	9.39
	−45 cm	18.00	51.00	12.00	143.00	74.00	37.00	75.20	24.00	248.00	4.15	336.00	43.40	88.20	9.04	31.50	6.20	1.27	5.28	0.76	4.38	0.82	2.38	0.34	2.30	0.33	6.11	2.30	23.40	7.81
	−50 cm	10.90	29.00	5.20	49.00	28.00	19.00	49.50	22.00	464.00	3.18	228.00	27.70	61.50	6.21	22.00	4.40	0.86	3.70	0.54	3.23	0.66	2.02	0.30	2.30	0.38	11.02	2.20	14.90	4.79
P3	−8 cm	20.30	65.00	15.90	126.00	92.00	56.00	79.30	27.00	110.00	5.25	360.00	51.00	105.70	10.79	39.20	7.70	1.69	6.67	0.96	5.42	1.04	2.92	0.41	2.70	0.40	3.26	2.80	27.00	10.08
	−16 cm	21.00	71.00	17.90	134.00	102.00	55.00	84.50	23.00	111.00	5.87	356.00	51.00	108.40	10.95	39.80	7.80	1.57	6.73	0.95	5.57	1.07	3.14	0.41	2.80	0.42	3.42	2.20	26.60	9.36
	−24 cm	20.10	135.00	130.90	122.00	79.00	50.00	82.30	22.00	116.00	5.83	367.00	51.70	110.10	11.4	40.20	7.90	1.58	6.62	0.91	5.09	1.02	2.97	0.39	2.80	0.38	3.47	2.30	27.60	8.42
	−32 cm	20.80	62.00	19.90	153.00	94.00	46.00	85.00	21.00	103.00	5.16	375.00	54.80	111.50	11.34	40.60	7.50	1.57	6.38	0.87	5.02	0.98	2.72	0.39	2.50	0.37	3.10	2.10	29.90	9.87
	−36 cm	19.70	70.00	32.20	145.00	93.00	46.00	88.80	23.00	5.55	5.55	54.20	54.20	41.00	11.25	7.50	1.63	0.90	6.66	0.90	5.21	1.00	2.82	0.39	0.39	0.39	1.44	2.50	8.70	8.70

UCC: upper continental crust; PAAS: Average Post-Archaean Australian Shale; NASC: Average North American Shale Composite; CC1 Chondrite.
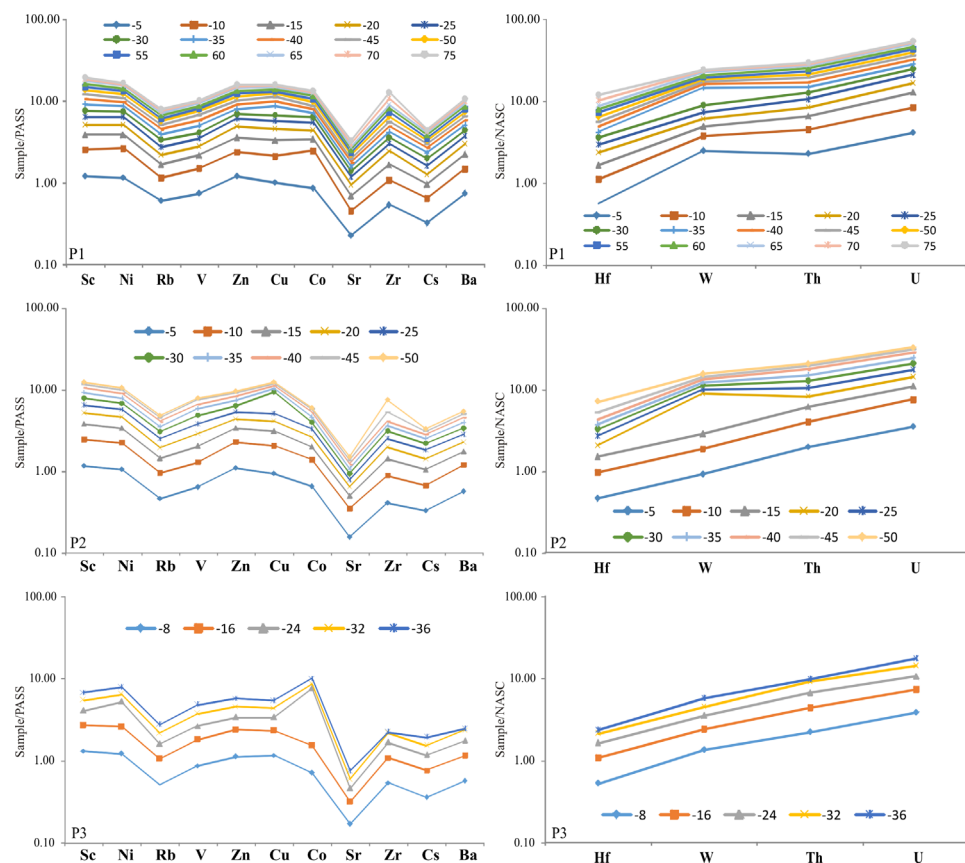
Figure 4. Trace element distribution for each sample normalized to Average Post-Archaean Australian Shale (PAAS) and Average North American Shale Composite (NASC) [46,53,55].
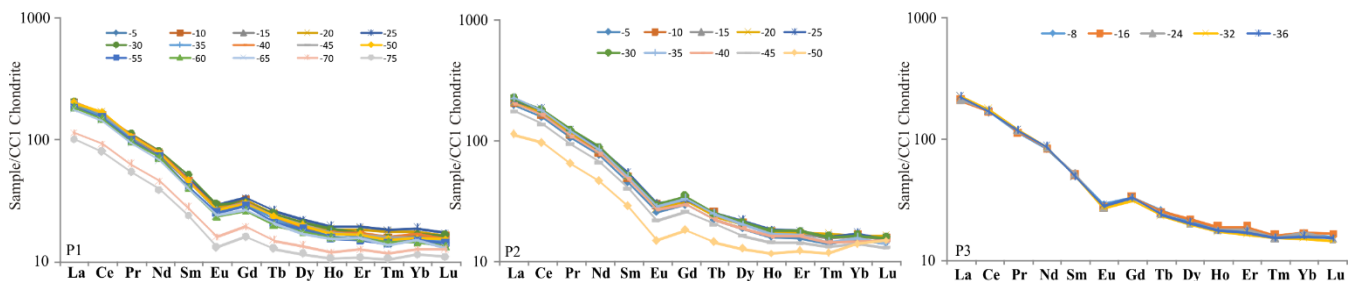

Figure 5. REE patterns for each sample normalized by the CC1 chondrite [47,48].

The Eu anomaly (Eu/Eu*) observed in all bottom sediments ranges from 0.78 to 0.65 with an average value of 0.71 (Figure 5 and Table 3), indicating that the Retiro Baixo sediments have a moderate anomaly that may result from a complex influence of plagioclase and heavy minerals and is usually interpreted as being inherited from igneous source rocks [1,2,61]. The bottom sediments present light rare-earth element (LREE) enrichment with a high La/Sm$_{cn}$ ratio, a negative Eu anomaly and an almost flat heavy rare-earth element (HREE) pattern with a low Gd/Yb$_{cn}$ ratio (Table 3).

As the REEs are concentrated in the more weathered strata, the sum of the REEs in each sample, as seen in Figure 6A (ΣREE vs. samples), shows the weathering degree in each profile and how they correlate among the riverbed sediment samples. Overall, all the upper samples present the highest REE concentrations, with the upper samples from P1 presenting an REE sum in the same magnitude order; in P2, there is an increase in the middle portion, and P3 presents corresponding values of REE sum in all profiles, thus indicating in each case their similarity in terms of weathering evolution.

Table 3. Bottom sediments trace element ratios in this study and international patterns for comparison.

		$(\Sigma REE)_{cn}$	$(\Sigma REE_L)_{cn}$	$(\Sigma REE_H)_{cn}$	$(La/Sm)_{cn}$	Eu/Eu*	$(Gd/Yb)_{cn}$	Co/Th	La/Sc
NASC		163.94	143.67	20.27	5.20	0.22	1.77	2.09	2.09
PASS		184.77	167.16	17.61	6.88	0.21	1.65	7.42	2.39
UCC		146.37	132.13	13.89	6.67	0.21	1.73	0.95	3.00
P1	−5 cm	742.53	596.59	146.20	4.21	0.70	1.24	0.73	2.51
	−10 cm	777.40	618.61	159.33	4.41	0.74	2.04	1.38	2.29
	−15 cm	750.22	594.59	155.55	4.09	0.78	1.94	0.91	2.18
	−20 cm	791.99	625.62	166.95	4.13	0.72	1.80	0.87	2.48
	−25 cm	798.92	623.62	175.50	4.04	0.72	1.84	1.03	2.42
	−30 cm	794.34	632.63	162.14	3.97	0.74	1.79	0.90	2.33
	−35 cm	760.79	609.60	151.58	4.32	0.71	1.83	0.73	2.08
	−40 cm	794.88	637.63	157.20	4.31	0.69	1.90	0.63	2.17
	−45 cm	780.23	624.62	155.34	4.47	0.72	1.83	0.64	2.18
	−50 cm	782.60	629.62	153.60	4.41	0.71	1.95	0.89	2.18
	−55 cm	718.04	575.57	142.23	4.48	0.73	1.91	0.95	2.07
	−60 cm	703.71	566.56	137.65	4.59	0.73	1.88	0.84	2.05
	−65 cm	682.57	545.54	137.12	4.41	0.74	1.80	0.83	1.75
	−70 cm	468.79	359.35	109.60	4.09	0.69	1.76	0.81	1.91
	−75 cm	407.23	312.31	94.83	4.24	0.67	1.53	0.61	2.17
P2	−5 cm	749.37	604.60	145.28	4.32	0.70	1.39	0.63	2.58
	−10 cm	805.11	643.64	161.23	4.21	0.74	1.95	0.68	2.40
	−15 cm	823.08	661.66	161.45	4.09	0.73	1.95	0.55	2.42
	−20 cm	812.72	652.65	160.03	4.18	0.69	1.98	0.55	2.24
	−25 cm	854.04	689.68	164.20	4.01	0.72	1.94	0.60	2.44
	−30 cm	865.45	700.70	165.13	4.34	0.70	1.92	0.56	2.55
	−35 cm	843.46	686.68	156.77	4.51	0.70	2.12	0.48	2.49
	−40 cm	780.30	633.63	147.28	4.27	0.72	2.11	0.54	2.24
	−45 cm	669.61	538.53	131.47	4.41	0.68	2.02	0.51	2.41
	−50 cm	473.58	363.36	109.66	3.96	0.65	1.86	0.35	2.54
P3	−8 cm	811.69	648.64	163.66	4.17	0.72	1.30	0.59	2.51
	−16 cm	821.30	653.65	167.53	4.12	0.66	2.00	0.67	2.43
	−24 cm	825.40	665.66	159.77	4.12	0.67	1.94	4.74	2.57
	−32 cm	830.78	677.67	152.83	4.60	0.69	1.91	0.67	2.63
	−36 cm	827.33	669.66	158.10	4.55	0.71	2.06	3.70	2.75

UCC: upper continental crust; PAAS: Average Post-Archaean Australian Shale; NASC: Average North American Shale Composite.
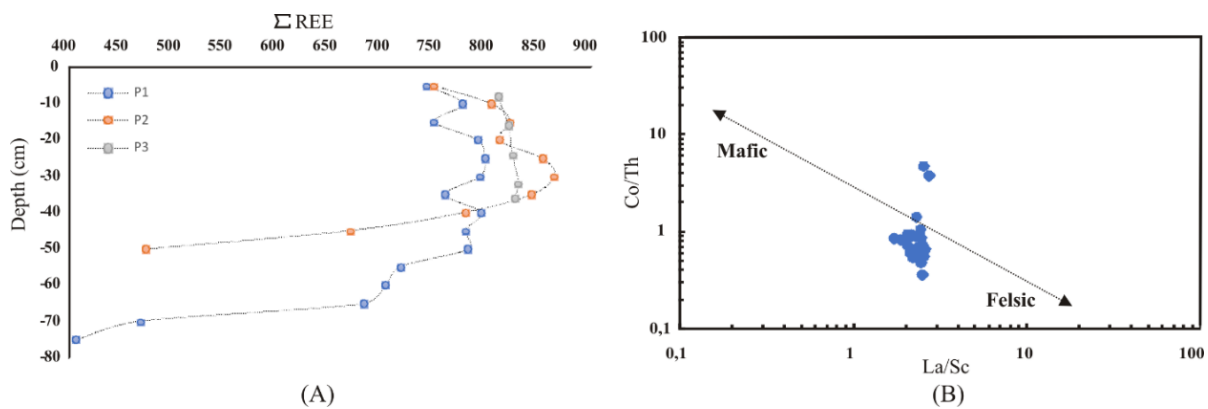

Figure 6. (**A**) REE sum (ΣREE) vs. sample depth. (**B**) Provenance discrimination diagrams of Co/Th vs. La/Sc.

The REEs and high-field-strength elements (HFSEs) are elements suitable for provenance analysis due to their relative sharp immobility during weathering, transport, dia-

genesis and metamorphism [60]. Refs. [2,53] suggested that REEs, Th, Sc and HFSEs are especially useful tools for plots of different compatible–incompatible element pairs, such as Co/Th vs. La/Sc, and have been used to differentiate felsic from mafic provenance. La and Th are immobile elements and are more abundant in felsic than basic rocks, whereas Sc and Co are more concentrated in basic rocks than in felsic rocks [53]. The Co/Th vs. La/Sc diagram for the bottom sediments is displayed in Figure 6B, where most of the samples fall in a region indicating a predominant intermediate source, which does not discard a felsic source or a mix of felsic and mafic sources (Figure 6B).

4.3. Environmental Impacts or Historical Accumulation

According to [26], extensive environmental monitoring is required to develop geochemical classification and a database. In this work, Figure 7 shows the vertical distribution for Si, Ti, Al, Fe, Mn, V, Co, Ni, Cu and Zn in bottom sediments, and Table 4 shows values from reference studies carried out for the upstream Córrego do Feijão Mine, Paraopeba River [52], average element concentrations of the 208 sediment samples from the Upper Velhas River in the Iron Quadrangle [12], the average for the 541 sediment samples from the whole Iron Quadrangle [38] and the intervention limits values established by Brazilian legislation [62].
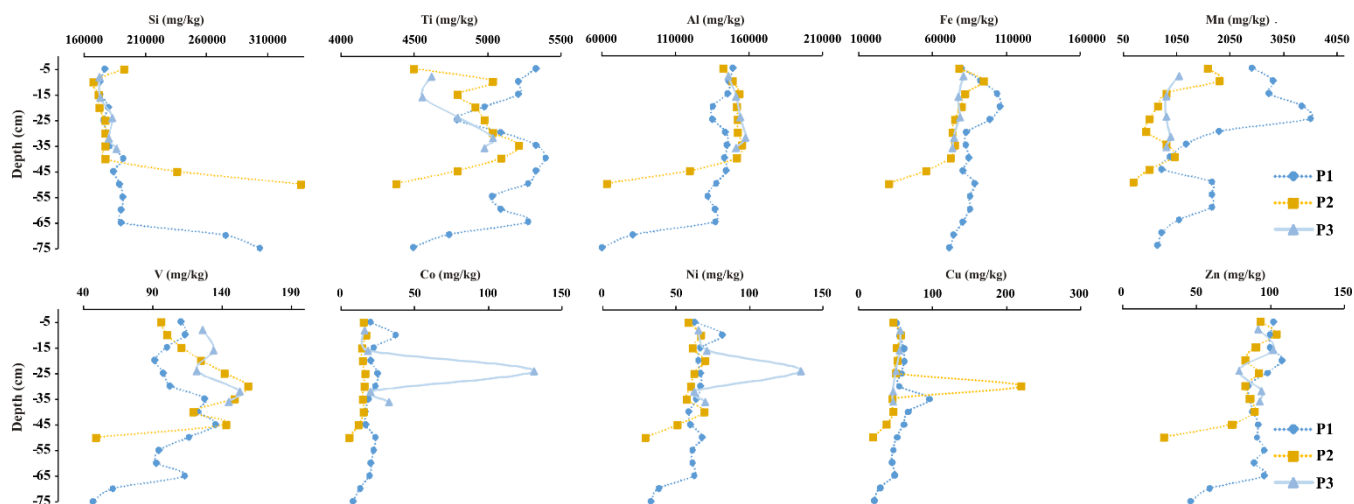

Figure 7. Major and trace element concentrations vs. depth of the sediment core.

Table 4. Chemical composition of major and trace elements (mg/kg) in reference studies and Probable Effect Level established by Brazilian legislation CONAMA 454/2012 [62].

	Si	Ti	Al	Fe	Mn	V	Co	Ni	Cu	Zn
[52]	335,200	4800	25,932	127,300	775	30	7	15	12	36
[52]	420,000	1800	11,700	40,600	775	13	11	11	8	27
[12]	--	--	13,230	90,230	1320	--	--	36	28	54
[38]	--	360	12,200	97,200	1600	--	15	38	23	51
[62]	--	--	--	--	--	--	--	35.90	197	315

The vertical distribution trends of the major and trace element concentrations were also investigated according to depth (Figure 7). The major and total trace element concentrations in the sediment core showed a greater abundance of Si, followed by Al, Fe, Ti, Mn, V, Zn, Ni, Cu and Co. The average concentrations of Al (P1 = 131,800 mg/kg, P2 = 139,210 mg/kg and P3 = 152,000 mg/kg), Ti (P1 = 5110 mg/kg and P2 = 4900 mg/kg), Mn (P1 = 1840 mg/kg) and Zn (P1 = 89 mg/kg, P2 = 82 mg/kg and P3 = 92 mg/kg) are higher than those obtained by authors who previously worked in the study region (Table 4). In addition, unlike the

behavior observed for Si, the Ti, Al, Fe, Mn and Zn concentrations increased from the deepest to the shallowest samples (Figure 7).

The total concentrations of Co, Ni and Cu are practically constant in the sediment core, with the following ranges: P1 = 37–8 mg/kg, 82–33 mg/kg and 95–20 mg/kg; P2 = 17–5 mg/kg, 70–29 mg/kg and 220–19 mg/kg; P3 = 131–16 mg/kg, 135–62 mg/kg and 56–46 mg/kg. However, Co (P3 = 131 mg/kg), Ni (P3 = 135 mg/kg), Cu (P2 = 220 mg/kg), Ti (P1 = 5400 mg/kg), Mn (P1 = 3600 mg/kg) and V (P2 = 160 mg/kg) presented temporal effects marked by higher total concentrations at the −35 cm and −25 cm depths compared with other samples, increasing their concentrations as observed for ∑REEs (Figures 5 and 6). In addition, most of the Ni samples showed values above those assigned by the current Brazilian legislation [62] (35.90 mg/kg—Table 4). According to [19], despite the elevated concentration of Ni, it does not mean that it has the potential to be released into water under river flow conditions; consequently, this reduces their accessibility to the food chain.

Table 5 shows minimum, maximum and mean values for contamination factor (CF), enrichment factor (EF) and geoaccumulation index (Igeo) obtained for the major and trace elements present in the sediment core. The CF was classified into four different classes [49]: low degree (CF ≤ 1), moderate degree (1 < CF ≤ 3), considerable degree (3 < CF < 6) and very high degree (CF ≤ 6). In addition, it was assumed that for EF ≤ 1.0, the contributions of the studied metals are natural and, for EF > 1.0, the contributions can be related to anthropogenic sources [19,24]. The Igeo was calculated by using the same background reference, indicating, according to [50], uncontaminated for Igeo < 1, moderate pollution for 1 < Igeo < 3, heavy pollution for 3 < Igeo < 5 and extreme pollution for Igeo > 5. The CF, EF and Igeo values for Si, Ti and Fe are < 1.0 along the sediment core, indicating a natural source for the contributions (Table 5).

Table 5. CF, EF and Igeo obtained for the major and trace elements for segments from the sampled sediment core (minimum, maximum and mean values) evaluated by comparing the collected data to a background in two sediment samples from the upstream Córrego do Feijão Mine, the Paraopeba River.

	CF						EF						Igeo					
	Min		Max		Mean		Min		Max		Mean		Min		Max		Mean	
Si	0.5	0.4	1.0	0.8	0.6	0.5	0.3	0.2	1.0	0.8	0.3	0.3	−1.6	−1.9	−0.6	−0.9	−1.4	−1.7
Ti	0.9	2.4	1.1	3.0	1.0	2.8	0.5	1.3	0.9	2.5	0.6	1.5	−0.7	0.7	−0.4	1.0	−0.5	0.9
Al	2.3	5.2	6.1	13.6	5.3	11.8	2.2	5.0	3.3	7.4	2.9	6.3	0.6	1.8	2.0	3.2	1.8	2.9
Fe	0.2	0.7	0.8	2.6	0.6	2.0	0.2	0.8	0.5	1.7	0.3	1.1	−2.7	−1.0	−0.8	0.8	−1.3	0.4
Mn	0.3	0.3	4.6	4.6	1.8	1.8	0.3	0.3	2.5	2.5	0.9	0.9	−2.3	−2.3	1.6	1.6	0.0	0.0
V	1.6	3.5	5.4	12.0	3.8	8.5	1.5	3.4	2.9	6.6	2.0	4.6	0.1	1.2	1.8	3.0	1.3	2.5
Co	0.7	0.5	18.7	12.3	3.1	2.1	0.7	0.5	10.2	6.8	1.7	1.1	−1.0	−1.6	3.6	3.0	0.8	0.2
Ni	1.9	2.6	8.8	11.9	4.1	5.6	1.8	2.4	4.8	6.5	2.2	3.0	0.3	0.8	2.5	3.0	1.4	1.9
Cu	1.5	2.5	17.9	28.6	4.5	7.2	1.6	2.5	9.1	14.6	2.4	3.8	0.0	0.7	3.6	4.3	1.5	2.1
Zn	0.8	1.1	3.0	4.1	2.4	3.3	0.8	1.1	1.7	2.3	1.3	1.8	−0.9	−0.5	1.0	1.4	0.65	1.1

Based on the contamination factor average values (CF—Equation (4)) and index (Table 5), the individual contamination levels in this reservoir are shown in the following sequence: Al > V > Cu > Ni > Zn > Ti > Co > Fe > Mn and Si. The CF values vary between 0.2 and 28.6, characterizing sediment with low to very high contamination degrees. Among the thirty samples of the sediment cores and considering these ten elements, the intermediate samples from the sediment cores presented moderate to considerable contamination degrees, marked by CF values of 28.6 for Cu at P2 (−30 cm), 18.7 for Co at P3 (−24 cm), 13.5 for Al at P3 (−32 cm), 12.0 for Ni at P3 (−24 cm), 12.0 for V at P2 (−30 cm), 4.6 for Mn at P1 (−25 cm), 4.1 for Zn at P1 (−20 cm) and 2.6 for Fe at P1 (−20 cm), thus characterizing the presence of the specified elements in the sediments probably due to anthropogenic activity sources.

The mean EF (Equation (5)) values in the sediment cores samples follow the same sequence presented for the CF values (Table 5). Al, V, Cu, Ni, Zn, Ti, Co, Fe and Mn EF

values in the segments are greater than 1 (>1.0), indicating that contributions can be related to anthropogenic sources. No enrichment is found for the Si element, which suggests their lithogenic origin as the predominant source for this element. For Mn, Zn and Fe the highest values are observed in the middle and deeper samples: 2.5 for P1 (−25 and −20 cm); 1.7 for P1 (−20 cm); and 1.7 for P1 (−75 cm). Compared with other sampling sites and depths, Cu, Al, Co and V reach extreme EF values (14.6, 7.4, 6.8 and 6.6, respectively) and maximum enrichment levels at P2 (−30 cm), P1 (−5 cm), P3 (−24 cm) and P2 (−45 cm), located in the central region or intermediate zone and close to the spillway or lake area, showing severe sediment enrichment, except for Al located close to the beginning or river zone in near-surface.

The geoaccumulation indexes (Equation (6)) obtained in the core samples are summarized in Table 5 and show a decreasing trend in the same order of that obtained for the CF and the EF. The calculated values range from −2.7 to 4.3, indicating uncontaminated to heavy pollution. According to the mean Igeo values of Si, Ti and Fe (Table 5), the sediments were considered uncontaminated by these elements. The mean geoaccumulation indexes of the remaining elements, such as Al, V, Cu, Ni and Zn, classify the sediments as moderately polluted (1 < Igeo < 2). Based on the maximum Igeo values, the sediments are considered heavily polluted with Cu (4.3) at P2 (−30 cm), Co and Cu (3.6) at P3 (−24 cm) and P2 (−30 cm), Al (3.2) at P3 (−32 cm), Ni and V (3.0) at P3 (−24 and −32 cm). Thus, the CF, EF and Igeo values of Al, Cu, Ni, V, Zn, Co and Mn suggest an anthropogenic influence on these elements' concentrations, but the sources or the human activities contributing to this concentrations remain to be assessed.

Reservoirs on a river system decrease flow velocity and turbulence and accumulate the sediment transported by runoff from upstream watersheds. The historical accumulation of major and trace elements in the Retiro Baixo reservoir reflects land-use land-cover changes, which could be due to mining, agricultural exploration, pastures, urban occupation, industrial and urban wastes, exposed soil and forestry. In addition, there is a complex geological framework, with mafic, ultramafic, gneissic, granitic, quartzite, phyllite, dolomite and itabirite rocks and sedimentary coverings, that is reflected in the main soil types—Ferralsols, Acrisols, Cambisols and others—which can contribute to transport from the upper region through streams, tributaries, etc.

In a study carried out after the collapse of the Fundão iron ore tailing dam in Quadrilatero Ferrífero [63], it was determined by using the Igeo that Ni and Zn were in the range between unpolluted and moderately polluted. After the failure of the Fundão tailing dam in seafloor sediments from the Espírito Santo Continental Shelf, [64] revealed a contamination of shelf sediments with Zn, Pb, Ni, Cr, Cu and Fe before the disaster, and a noticeable increase in Zn and Fe concentrations after the dam failure. According to [65], the concentrations of Al, Fe and Mn in bauxite mine-impacted water were slightly higher, while the concentrations of Cu and Zn in sediments were high at some sampling locations; however, apart from the mining activities, the contribution of Zn in agricultural soils might have promoted the concentration of Cu in sediment.

In the Três Marias reservoir, according to [66], Ti, Zn and Cu are related to the lithotypes from ultramafic rocks and sedimentary covers from the Bambuí Group and anthropogenic sources correlated with forestry and agriculture associated with the use of pesticides. Also, anthropogenic inputs of Co and Ni can be associated to agricultural practices (fertilizers and pesticides), and Zn can be charged by domestic/urban sewage and industrial effluents [6,61,65,67,68].

The Al, Cu, Ni, V, Zn, Co, Mn, Ti, Fe and Si concentrations and the CF, EF and Igeo index values vary across the sediment core samples, demonstrating that there are geogenic or anthropogenic contributions. The urban agglomerations (domestic sewage and the dumping of untreated solid waste), agricultural exploitation (application of fertilizers and pesticides), geochemical background (relief, lithology and soil) and mining activities, as well as metallurgical, automobile and petrochemical industries, in the Paraopeba River basin can all contribute to the concentration of these elements in the bottom sediments. Thus, no major anomalies

were observed in the surface layers of bottom sediments in the Retiro Baixo reservoir, built between 1973 and 1981, despite the recent rupture of the B1 dam in Brumadinho, even after comparing our data to those of other studies prior to the rupture.

5. Conclusions

The study area is inserted in a complex geological and thus geochemical background that has been historically intervened upon by human activities such as the steel industry, metallurgical and automotive industries, agriculture, livestock farming and mining, so any considerations must be analyzed with caution. The rupture of the B1 dam at Brumadinho on 01/25/2019 released around 10 million cubic meters of waste, which eventually reached the Paraopeba River (our object of study), had worldwide repercussions and encouraged the need for studies on possible impacts derived from this major event.

After analyzing a total of 30 samples at three different locations at various depths in the riverbed sediments from the lower course of the Paraopeba River basin, by using several methods and by comparing our data to previous studies, our analysis did not show significant anomalies in the composition of sediments at various depths indicating multifactorial inputs. Thus, our study will serve as a basis for future analyses that are being and will be carried out in the study area, including the geochronology dating of the sediment core at various depths, which will bring forth more considerations regarding the variation in the major, rare-earth and trace elements' concentrations over time and the possible external factors associated.

Author Contributions: Field work, sample collection and preparation, G.B., D.A.S.d.M., D.S.S. and J.T.S.; investigation, methodology and validation, D.S.S., M.S.P., J.T.S., L.H.G., G.B., P.H.B.J.M., D.A.S.d.M. and F.V.L.; writing—original draft, D.S.S., L.H.G. and F.V.L.; writing—review and editing, D.S.S., L.H.G. and F.V.L. All authors have read and agreed to the published version of the manuscript.

Conflicts of Interest: Authors declare that the research was conducted in the absence of any commercial or financial relationships that could be construed as a potential conflict of interest. The conclusions present in this manuscript are the authors' consensual interpretation from the obtained data and literature review. Despite the research was funded by Vale and one co-author is a Vale employee, the authors declare no influence from the company on data reporting and discussion.

References

1. Wu, W.; Xu, S.; Lu, H.; Yang, J.; Yin, H.; Liu, W. Mineralogy, major and trace element geochemistry of riverbed sediments in the headwaters of the Yangtze, Tongtian River and Jinsha River. *J. Asian Earth Sci.* **2011**, *40*, 611–621. [CrossRef]
2. Wu, W.; Zheng, H.; Xu, S.; Yang, J.; Liu, W. Trace element geochemistry of riverbed and suspended sediments in the upper Yangtze River. *J. Geochem. Explor.* **2013**, *124*, 67–78. [CrossRef]
3. Zhang, K.; Peng, B.; Yang, X. Contamination and Risk of Heavy Metals in Sediments from Zhuzhou, Xiangtan and Changsha Sections of the Xiangjiang River, Hunan Province of China. *Sustainability* **2023**, *15*, 14239. [CrossRef]
4. Wang, S.; Wang, Y.; Zhang, R.; Wang, W.; Xu, D.; Guo, J.; Li, P.; Yu, K. Historical levels of heavy metals reconstructed from sedimentary record in the Hejiang River, located in a typical mining region of southern China. *Sci. Total Environ.* **2015**, *532*, 645–654. [CrossRef] [PubMed]
5. Martín-Crespo, T.; Gómez-Ortiz, D.; Martín-Velázquez, S.; Martínez-Pagán, P.; De Ignacio, C.; Lillo, J.; Faz, Á. Geoenvironmental characterization of unstable abandoned mine tailings combining geophysical and geochemical methods (Cartagena-La Union district, Spain). *Eng. Geol.* **2018**, *232*, 135–146. [CrossRef]
6. Martín-Crespo, T.; Gómez-Ortiz, D.; Martín-Velázquez, S.; Martínez-Pagán, P.; De Ignacio, C.; Lillo, J.; Faz, Á. Abandoned mine tailings affecting riverbed sediments in the Cartagena–La Union district, mediterranean coastal area (Spain). *Remote Sens.* **2020**, *12*, 2042. [CrossRef]

7.   Sánchez-Donoso, R.; García Lorenzo, M.L.; Esbrí, J.M.; García-Noguero, E.M.; Higueras, P.; Crespo, E. Geochemical characterization and trace-element mobility assessment for metallic mine reclamation in soils affected by mine activities in the iberian pyrite belt. *Geosciences* **2021**, *11*, 233. [CrossRef]

8.   Azizi, M.; Faz, A.; Zornoza, R.; Martínez-Martínez, S.; Shahrokh, V.; Acosta, J.A. Environmental pollution and depth distribution of metal(loid)s and rare earth elements in mine tailing. *J. Environ. Chem. Eng.* **2022**, *10*, 107526. [CrossRef]

9.   Rodríguez-Pacheco, R.; Caparrós, A.V.; Alcolea, A.; Martínez-Pagán, P.; Martínez-Segura, M.A.; García-García, C.; Faz, Á.; Corral, I.; Roque, C.; Zarroca, M. Static Liquefaction Causes the Flow Failure of a Tailings Dam: A Case Study of El Descargador, Cartagena–La Unión Mining Region, SE Spain (October 1963). *Minerals* **2022**, *12*, 1488. [CrossRef]

10. Salhi, R.; Durães, N.; Dhaoui, M.; Patinha, C.; da Silva, E.F.; Mlayah, A. Contamination assessment and availability of potential toxic elements from the Sidi Driss tailing pile (NW Tunisia) based on geochemical and geophysical methods. *J. Afr. Earth Sci.* **2023**, *202*, 104921. [CrossRef]

11. Sayom, R.Y.A.; Mfenjou, M.L.; Ngounouno, M.A.; Etoundi, M.M.C.; Boroh, W.A.; Ngueyep, L.L.M.; Meying, A. A coupled geostatistical and machine learning approach to address spatial prediction of trace metals and pollution indices in sediments of the abandoned gold mining site of Bekao, Adamawa, Cameroon. *Heliyon* **2023**, *9*, e18511. [CrossRef] [PubMed]

12. Vicq, R.; Leite, M.G.P.; Leão, L.P.; Nallini Júnior, H.A.; Valente, T. Geochemical Mapping and Reference Values of Potentially Toxic Elements in a Contaminated Mining Region: Upper Velhas River Basin Stream Sediments, Iron Quadrangle, Brazil. *Minerals* **2023**, *13*, 1545. [CrossRef]

13. Zhang, H.; Wang, X.; Wang, H.; Yin, J.; Wang, R.; Shi, Z.; Ni, S. Distribution of Uranium and Molybdenum in River Sediment near Molybdenite Mining Region: A Case Study in SW China. *Minerals* **2023**, *13*, 1435. [CrossRef]

14. Onnis, P.; Byrne, P.; Hudson-Edwards, K.A.; Stott, T.; Hunt, C.O. Fluvial Morphology as a Driver of Lead and Zinc Geochemical Dispersion at a Catchment Scale. *Minerals* **2023**, *13*, 790. [CrossRef]

15. Kríbek, B.; Nyambe, I.; Sracek, O.; Mihaljevič, M.; Knésl, I. Impact of Mining and Ore Processing on Soil, Drainage and Vegetation in the Zambian Copperbelt Mining Districts: A Review. *Minerals* **2023**, *13*, 384. [CrossRef]

16. Beres, I.; Maftei, A.E.; Dill, H.G.; Buzatu, A.; Damian, G. Contamination Assessment of Toxic Elements in River Sediments from Baia Mare, Romania—Extreme Pollution from Mining Activities. *Minerals* **2024**, *14*, 135. [CrossRef]

17. Sánchez, L.E.; Alger, K.; Alonso, L.; Barbosa, F.A.R.; Brito, M.C.W.; Laureano, F.V.; May, P.; Roeser, H.; Kakabase, Y. *Impacts of the Fundão Dam Failure. A Pathway to Sustainable and Resilient Mitigation*; Rio Doce Panel Thematic Report; IUCN: Gland, Switzerland, 2018. [CrossRef]

18. Keim, C.N.; Serna, J.D.P.; Acosta-Avalos, D.; Neumann, R.; Silva, A.S.; Jurelevicius, D.A.; Pereira, R.S.; de Souza, P.M.; Seldin, L.; Farina, M. Dissimilatory Iron-Reducing Microorganisms Are Present and Active in the Sediments of the Doce River and Tributaries Impacted by Iron Mine Tailings from the Collapsed Fundão Dam (Mariana, MG, Brazil). *Minerals* **2021**, *11*, 244. [CrossRef]

19. Conceição, F.T.; Fernandes, A.M.; Hissler, C.; Lupinacci, C.M.; Menegário, A.M.; Moruzzi, R.B. Multi-tracer analysis to estimate the historical evolution of pollution in riverbed sediment of subtropical watershed, the lower course of the Piracicaba River, São Paulo, Brazil. *Sci. Total Environ.* **2020**, *743*, 140730. [CrossRef] [PubMed]

20. Vauclin, S.; Mourier, B.; Dendievel, A.M.; Noclin, N.; Piégay, H.; Marchand, P.; Vénisseau, A.; de Vismes, A.; Lefèvre, I.; Winiarski, T. Depositional environments and historical contamination as a framework to reconstruct fluvial sedimentary evolution. *Sci. Total Environ.* **2021**, *764*, 142900. [CrossRef]

21. Meybeck, M.; Lestel, L.; Bonte, P.; Moilleron, R.; Colin, J.L.; Rousselot, O.; Herve, D.; de Ponteves, C.; Thevenot, D.R. Historical perspective of heavy metals contamination (Cd, Cr, Cu, Hg, Pb, Zn) in the Seine River basin (France) following a DPSIR approach (1950–2005). *Sci. Total Environ.* **2007**, *375*, 204–231. [CrossRef]

22. Mortatti, J.; Moraes, G.M.; Probst, J.L. Heavy metals distribution in recent sediments along the Tietê River basin (São Paulo, Brazil). *Geochem. J.* **2012**, *46*, 13–19. [CrossRef]

23. Zahra, A.; Hashmi, M.Z.; Malik, R.N.; Ahmed, Z. Enrichment and geo-accumulation of heavy metals and risk assessment of sediments of the Kurang Nallah-feeding tributary of the Rawal Lake reservoir. Pakistan. *Sci. Total Environ.* **2014**, *470–471*, 925–933.

24. Fernandes, A.M.; Hissler, C.; Conceição, F.T.; Spatti Junior, E.P.; Mortatti, J. Combined analysis of trace elements and isotopic composition of particulate organic matter in suspended sediment to assess their origin and flux in a tropical disturbed watershed. *Environ. Pollut.* **2016**, *218*, 844–854. [CrossRef] [PubMed]

25. Ledru, M.; Jeske-Pieruschka, V.; Bremond, L.; Develle, A.; Sabatier, P.; Martins, E.S.P.R.; Freitas Filho, M.R.; Fontenele, D.P.; Arnaud, F.; Favier, C.; et al. When archiver are missing, deciphering the effects of public policies and climate variability on the Brazilian semi-arid region using sediment core studies. *Sci. Total Environ.* **2020**, *723*, 137989. [CrossRef] [PubMed]

26. Nawrot, N.; Wojciechowska, E.; Mohsin, M.; Kuittinen, S.; Pappinen, A.; Rezania, S. Trace Metal Contamination of Bottom Sediments: A Review of Assessment Measures and Geochemical Background Determination Methods. *Minerals* **2021**, *11*, 872. [CrossRef]

27. Moldovan, A.; Török, A.I.; Kovacs, E.; Cadar, O.; Mirea, I.C.; Micle, V. Metal Contents and Pollution Indices Assessment of Surface Water, Soil, and Sediment from the Aries, River Basin Mining Area, Romania. *Sustainability* **2022**, *14*, 8024. [CrossRef]

28. Ferreira, S.L.C.; da Silva Junior, J.B.; dos Santos, I.F.; de Oliveira, O.M.C.; Cerda, V.; Queiroz, A.F.S. Use of pollution indices and ecological risk in the assessment of contamination from chemical elements in soils and sediments—Practical aspects. *Trends Environ. Anal. Chem.* **2022**, *35*, e00169. [CrossRef]

29. Shevchenko, V.P.; Starodymova, D.P.; Vorobyev, S.N.; Aliev, R.A.; Borilo, L.P.; Kolesnichenko, L.G.; Lim, A.G.; Osipov, A.I.; Trufanov, V.V.; Pokrovsky, O.S. Trace Elements in Sediments of Two Lakes in the Valley of the Middle Courses of the Ob River (Western Siberia). *Minerals* **2022**, *12*, 1497. [CrossRef]

30. Ahirvar, B.P.; Das, P.; Srivastava, V.; Kumar, M. Perspectives of heavy metal pollution indices for soil, sediment, and water pollution evaluation: An insight. *Total Environ. Res. Themes* **2023**, *6*, 100039. [CrossRef]

31. Popoola, S.O.; Nubi, A.O.; Unyimadu, J.P.; Ladigbolu, I.A.; Fabunmi, I.; Udochu, U.; Nwamba, E.; Oba, I.A.; Mordi, S.; Adamu, S. Pollution indices and ecological risk assessment of major elements and trace metals in the marine sediment of the western Nigeria continental shelf, Gulf of Guinea. *Sci. Afr.* **2023**, *22*, e01923. [CrossRef]

32. Vaezi, A.; Lak, R. Sediment Texture, Geochemical Variation, and Ecological Risk Assessment of Major Elements and Trace Metals in the Sediments of the Northeast Persian Gulf. *Minerals* **2023**, *13*, 850. [CrossRef]

33. Rong, S.; Wu, J.; Liu, J.; Li, Q.; Ren, C.; Cao, X. Environmental Magnetic Characteristics and Heavy Metal Pollution Assessment of Sediments in the Le'an River, China. *Minerals* **2023**, *13*, 145. [CrossRef]

34. Laureano, F.V.; Kwitko-Ribeiro, R.; Guimarães, L.; Leão, L.P. Mineralogical Fingerprint of Iron Ore Tailings in Paraopeba River Bedload Sediments after the B1 Dam Failure in Brumadinho, MG (Brazil). *Minerals* **2022**, *12*, 716. [CrossRef]

35. Kobayashi, H.; Garnier, J.; Mulholland, D.S.; Quantin, C.; Haurine, F.; Tonha, M.; Joko, C.; Olivetti, D.; Freydier, R.; Seyler, P.; et al. Exploring a new approach for assessing the fate and behavior of the tailings released by the Brumadinho dam collapse (Minas Gerais, Brazil). *J. Hazard. Mater.* **2023**, *448*, 130828. [CrossRef] [PubMed]

36. CBHSF. Comitê da Bacia Hidrográfica do Rio São Francisco. *CBH do Rio Paraopeba (SF3)—Minas Gerais.* 2019. Available online: http://cbhsaofrancisco.org.br/2017/comites-de-afluentes/cbh-do-rio-paraopeba-minas-gerais (accessed on 7 February 2019).

37. Alkmim, F.F.; Marshak, S. Transamazonian orogeny in the Southern Sao Francisco craton region, Minas Gerais, Brazil: Evidence for Paleoproterozoic collision and collapse in the Quadrilátero Ferrífero. *Precambrian Res.* **1998**, *90*, 29–58. [CrossRef]

38. Vicq, R.; Matschullat, J.; Leite, M.G.P.; Nallini Júnior, H.A.; Mendonça, F.P.C. Iron Quadrangle stream sediments, Brazil: Geochemical maps and reference values. *Environ. Earth Sci.* **2015**, *74*, 4407–4417. [CrossRef]

39. CPRM. *Companhia de Pesquisa de Recursos Minerais—Superintendência Regional de Belo Horizonte. Regionalização de Vazões Sub-Bacias 40 e 41, Convênio 015/2000 ANEEL—013/CPRM/2000, Relatório Final*; CPRM: Belo Horizonte, Brazil, 2001; 135p.

40. CPRM. *Companhia de Pesquisa de Recursos Minerais, Mapa Geológico. Escala 1:1.000.000*; CPRM: Belo Horizonte, Brazil, 2020.

41. UFV. *Universidade Federal de Viçosa, Fundação Centro Tecnológico de Minas Gerais; Universidade Federal de Lavras; Fundação Estadual do Meio Ambiente*; Fundação Estadual do Meio Ambiente: Belo Horizonte, Brazil, 2010; 49p.

42. Gomes, M.A. Caracterização Tecnológica no Aproveitamento do Rejeito de Minério de Ferro. Master's Thesis, Mineral Engineering Department, Federal University of Ouro Preto, Ouro Preto, Brazil, 2009.

43. Pacheco, F.A.L.; Valle Junior, R.F.; Melo Silva, M.M.A.P.; Pissarra, T.C.T.; Melo, M.C.; Valera, C.A.; Fernandes, L.S.F. Prognosis of metal concentrations in sediments and water of Paraopeba River following the collapse of B1 tailings dam in Brumadinho (Minas Gerais, Brazil). *Sci. Total Environ.* **2022**, *809*, 151157. [CrossRef]

44. Harnois, L. The CIW index: A new chemical index of weathering. *Sediment. Geol.* **1988**, *55*, 322. [CrossRef]

45. Cox, R.; Lowe, D.R.; Cullers, R.L. The influence of sediment recycling and basement composition on evolution of mudrock chemistry in the southwestern United States. *Geochim. Cosmochim. Acta* **1995**, *59*, 2919–2940. [CrossRef]

46. Gromet, L.P.; Dymek, R.F.; Haskin, L.A.; Korotev, R.L. The "North American shale composite": Its compilation, major and trace element characteristics. *Geochim. Cosmochim. Acta* **1984**, *48*, 2469–2482. [CrossRef]

47. Evensen, N.M.; Hamilton, P.J.; O'nions, R.K. Rare-earth abundances in chondritic meteorites. *Geochim. Cosmochim. Acta* **1978**, *42*, 1199–1212. [CrossRef]

48. Sun, S.S.; McDonough, W.F. Chemical and isotopic systematics of oceanic basalts: Implications for mantle composition and processes. *Geol. Soc. Spec. Publ.* **1989**, *42*, 313–345.

49. Håkanson, L. An ecological risk index for aquatic pollution control. a sedimentological approach. *Water Res.* **1980**, *14*, 975–1001. [CrossRef]

50. Müller, G. Index of geoaccumulation in sediments of the Rhine River. *Geo J.* **1969**, *2*, 108–118.

51. Shotyk, W.; Blaser, P.; Grüning, A.; Cheburkin, A.K. A new approach for quantifying cumulative, anthropogenic, atmospheric lead deposition using peat cores from bogs: Pb in eight Swiss peat bog profiles. *Sci. Total Environ.* **2000**, *249*, 281–295. [CrossRef] [PubMed]

52. Silva, L.S.C.; Picanço, J.L.; Pereira, C.C.; Silva, D.; Almeida, T.N. Dispersion of tailings in the Paraopeba River system after Brumadinho dam failure: Brazil. *Environ. Earth Sci.* **2024**, *83*, 128. [CrossRef]

53. Taylor, S.R.; McLennan, S.M. *The Continental Crust: Its Composition and Evolution*; Blackwell Scientific Publications: Oxford, UK, 1985; 312p, ISBN 0 632 01148 3.

54. Taylor, S.R.; McLennan, S.M. The geochemical evolution of the continental crust. *Rev. Geophys.* **1995**, *33*, 241–265. [CrossRef]

55. Morgan, J.W.; Higuchi, H.; Takahashi, H.; Hertogen, J. Chondritic Eucrite Parent Body-Inference from Trace-Elements. *Geochim. Cosmochim. Acta* **1978**, *42*, 27–38. [CrossRef]

56. Nesbitt, H.W.; Young, G.M. Early Proterozoic climates and plate motions inferred from major element chemistry of lutites. *Nature* **1982**, *299*, 715–717. [CrossRef]

57. Nesbitt, H.W.; Young, G.M. Prediction of some weathering trends of plutonic and volcanic rocks based on thermodynamic and kinetic considerations. *Geochim. Cosmochim. Acta* **1984**, *48*, 1523–1534. [CrossRef]

58. Nesbitt, H.W.; Young, G.M. Formation and diagenesis of weathering profiles. *J. Geol.* **1989**, *97*, 129–147. [CrossRef]

59. Herron, M.M. Geochemical classification of terrigenous sands and shales from core or log data. *J. Sediment. Res.* **1988**, *58*, 820–829. [CrossRef]

60. Godoy, L.H.; Sardinha, D.S.; Moreno, M.M.T. Major and trace elements redistribution in weathered claystones from the Corumbataí Formation, Paraná Sedimentary Basin, São Paulo, Brazil. *Braz. J. Geol.* **2017**, *47*, 615–632. [CrossRef]

61. Benabdelkader, A.; Talebb, A.; Probst, J.L.; Belaidib, N.; Probst, A. Origin, distribution, and behaviour of rare earth elements in river bed sediments from a carbonate semi-arid basin (Tafna River, Algeria). *Appl. Geochem.* **2019**, *106*, 96–111. [CrossRef]

62. Brazil. *Conselho Nacional do Meio Ambiente, CONAMA. Resolução 454, de 01 de Novembro de 2012. Estabelece as Diretrizes Gerais e os Procedimentos Referenciais Para o Gerenciamento do Material a ser Dragado em Águas Sob Jurisdição Nacional*; CONAMA: Brasília/DF, Brazil, 2012.

63. Duarte, E.B.; Neves, M.A.; Oliveira, F.B.; Martins, M.E.; Oliveira, C.H.R.; Burak, D.L.; Orlando, M.T.D.; Rangel, C.V.G.T. Trace metals in Rio Doce sediments before and after the collapse of the Fundao iron ore tailing dam, Southeastern Brazil. *Chemosphere* **2021**, *262*, 127879. [CrossRef] [PubMed]

64. Quaresma, V.S.; Aguiar, V.M.C.; Bastos, A.C.; Oliveira, K.S.; Vieira, F.V.; Sá, F.; Baptista Neto, J.A. The impact of trace metals in marine sediments after a tailing dam failure: The Fundão dam case (Brazil). *Environ. Earth Sci.* **2021**, *80*, 571. [CrossRef]

65. Kusin, F.M.; Rahman, M.S.A.; Madzin, Z.; Jusop, S.; Mohamat-Yusuff1, F.; Ariffin, M.; Syakirin, M. The occurrence and potential ecological risk assessment of bauxite mine-impacted water and sediments in Kuantan, Pahang, Malaysia. *Environ. Sci. Pollut. Res. Int.* **2017**, *24*, 1306–1321. [CrossRef] [PubMed]

66. Lima, G.F.C.; Bento, C.C.; Horn, A.H.; Marques, E.D.; Baggio Filho, H. Seasonal geochemical trends and pollution assessment of bottom sediments in the São Francisco hydrographic basin, Brazil: The Três Marias Reservoir. *Environ. Sci. Pollut. Res.* **2022**, *29*, 42929–42946. [CrossRef] [PubMed]

67. Mortatti, J.; Oliveira, H.; Moraes, G.M.; Vendramini, D.; Fernandes, A.M. Distribution of heavy metals in the geochemical phases of sediments from the Tietê River, Brazil. *Chem. Speciat. Bioavailab.* **2013**, *25*, 3. [CrossRef]

68. Shang, G.; Wang, X.; Zhu, L.; Liu, S.; Li, H.; Wang, Z.; Wang, B.; Zhang, Z. Heavy Metal Pollution in Xinfengjiang River Sediment and the Response of Fish Species Abundance to Heavy Metal Concentrations. *Int. J. Environ. Res. Public Health* **2022**, *19*, 11087. [CrossRef]